QUASI-STATIC NORMAL INDENTATION OF AN ELASTO-PLASTIC HALF-SPACE BY A RIGID CIRCULAR CYLINDER OF INFINITE LENGTH

A. CINAR

Department of Civil Engineering, Technical University of Istanbul, Istanbul, Turkey

and

G. B. SINCLAIR†

Department of Mechanical Engineering, Carnegie-Mellon University, Pittsburgh, PA 15213, U.S.A.

Abstract—The title problem is treated under the conditions of frictionless and completely adhesive contact within the context of incremental elasto-plasticity. The analysis employs a constant-strain-triangle, finite element code, together with a grid expansion technique which aids computational efficiency. Attendant results are checked where possible then processed to furnish: the indentation extent with increasing pressure, the contact and interior stresses on loading and unloading, yield region growth, and relative displacement profiles at the surface. Comparisons with related experiments in the literature are made and generally show reasonable agreement.

INTRODUCTION

The *contact problem* of concern here considers the stresses and deformations that accumulate when a circular cylinder of indefinite length is slowly pressed normally into a relatively soft half-space. This configuration represents the plane strain analogue of the axisymmetric, spherical, indentation problem—the Brinell hardness test in effect. As such, its obvious physical significance is less, though it does contain information of some practical importance. Specifically, at low load levels it provides inferences regarding wear in roller bearings, while at higher indenting pressures it has implications for the shakedown of a half-space under repeated trackings of a ball across its surface. As well plane, strain, normal indentation constitutes a first step in the study of the plane problem of *inclined* indentation, the latter being planned as an analytically feasible means of inferring the effects of off-normal impact in the erosive wear model of Follansbee *et al.*[1]. In all then, the subject contact problem merits some attention.

Probably the earliest contribution to the problem is contained in Hertz's classical elastostatic treatment[2]. Detailed calculations for the elastic response can be found in Poritsky[3]. In a number of practical cases, however, the indentation is such that considerable yielding is induced in the half-space, limiting the value of the elastic solution. Accordingly, there is a need to track the associated plastic flow. The simplest approach to this end would seem to be slip-line theory, assuming a rigid/perfectly plastic half-space. Such an analysis does not seem to be available in the literature, possibly because uniqueness difficulties arise in constructing the slip-line fields.‡ A more physically realistic approach is to use the theory of incremental elasto-plasticity which includes both elastic and plastic deformation and has the additional attribute of admitting strain-hardening. Unfortunately, these improvements are at the expense of tractability, so that attempts reported to analyze the problem within this theory are numerical, for the most part using the finite element

---

† To whom correspondence should be addressed.

‡ There are some slip-line treatments of rolling cylinder contact which might appear to be relevant, e.g. Collins[4]. By virtue of the fact that [4] and like analyses treat the chord of the portion of the cylinder in contact as the actual contact surface, these problems are no more pertinent to the present investigation than the plane strain indentation of a half-space by a flat punch, the slip-line solution for which being first given by Prandtl, and described and modified by Hill[5], pp. 245 and 246.

method; see Dumas and Baronet[6] and references therein. Even with recourse to numerical methods the problem resists solution. Dumas and Baronet[6] use finite elements with a fine grid which captures the key field quantities with sufficient resolution but which, because of the attendant computational effort, severely limits the extent to which the half-space can be loaded in excess of the elastic limit. Our objective here is to treat the problem within incremental elasto-plasticity with a finite element grid of sufficient resolution and accuracy, yet to take the calculations through to the point of including the upper load levels encountered in applications. In taking these calculations further we are aided by a new generation of computers since Dumas and Baronet[6] and by the simple but effective expansion technique of Follansbee and Sinclair[7]; this last maintains resolution while reducing computation times by about an order of magnitude.

We begin in Section 1 by formulating the problem considered and describing how the analysis is carried out. Next in Section 2, we first discuss results found with a view to validating the approach, then present other results felt to be of physical importance and compare them with experimental counterparts in the literature (the Appendix provides a measure of accompanying numerical noise).

1. FORMULATION AND ANALYSIS

Here we set down a class of problems which addresses the determination of the stresses, strains and displacements that accumulate in an initially undisturbed, elasto-plastic half-space when an infinitely long, rigid cylinder is slowly pressed normally into its surface. We then specialize this class to a particular material, a prerequisite to numerical analysis. Finally, we describe the finite element analysis adopted and the means used to reduce the resulting data.

To formulate the problem class, let (x, y, z) be rectangular cartesian coordinates with origin O such that the surface of the half-space $\mathcal{H}$ is formed by the xz-plane with y positive into $\mathcal{H}$ (Fig. 1). Thus

$$\mathcal{H} = \{(x, y, z)|\, |x| < \infty, \quad 0 < y < \infty, \quad |z| < \infty\}. \tag{1.1}$$

At some time $t > 0$, an infinitely long, rigid, circular cylinder of radius R indents the half-space under a force F per unit of its length, forming an infinitely long strip of contact of
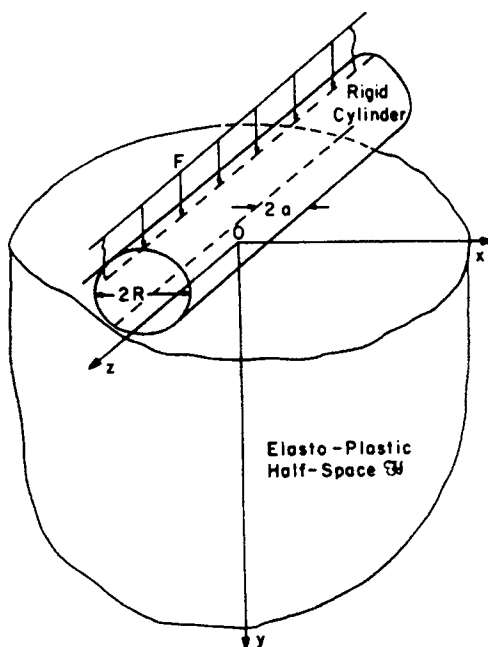

Fig. 1. Configuration and coordinates.

width $2a$ centered on the z-axis. That is, if $\partial_1\mathcal{H}$ is the contact region and $\partial_2\mathcal{H}$ the half-space surface free from contact, we have

$$\partial_1\mathcal{H} = \{(x, y, z)| \, |x| < a, \quad y = 0, \quad |z| < \infty\},$$
$$\partial_2\mathcal{H} = \{(x, y, z)| \, |x| > a, \quad y = 0, \quad |z| < \infty\}. \tag{1.2}$$

The problem is one of *plane strain* in the z-direction, viz., no displacements in the z-direction and $\partial/\partial z$ a null operator on $\mathcal{H}$ for all time. We seek, therefore, the stresses $\sigma = (\sigma_x, \sigma_y, \sigma_z, \tau_{xy})$, strains $\varepsilon = (\varepsilon_x, \varepsilon_y, \gamma_{xy})$ and displacements $u = (u, v)$, as functions of x, y alone throughout $\mathcal{H}$ for all time $t > 0$, resulting from the accumulation of their corresponding rates in accordance with

$$\sigma = \int_0^t \dot{\sigma} \, dt, \qquad \varepsilon = \int_0^t \dot{\varepsilon} \, dt, \qquad u = \int_0^t \dot{u} \, dt, \tag{1.3}$$

on $\mathcal{H}$, wherein the rate quantities $\dot{\sigma} = (\dot{\sigma}_x, \dot{\sigma}_y, \dot{\sigma}_z, \dot{\tau}_{xy})$, $\dot{\varepsilon} = (\dot{\varepsilon}_x, \dot{\varepsilon}_y, \dot{\gamma}_{xy})$, $\dot{u} = (\dot{u}, \dot{v})$ are to satisfy the following requirements.[†] The plane strain, stress-rate *equations of equilibrium* in the absence of body forces under the assumption of quasi-static response,

$$\partial\dot{\sigma}_x/\partial x + \partial\dot{\tau}_{xy}/\partial y = 0, \qquad \partial\dot{\sigma}_y/\partial y + \partial\dot{\tau}_{xy}/\partial x = 0, \tag{1.4}$$

on $\mathcal{H}$ for $t > 0$. The *flow rule* for a homogeneous and isotropic, elastic/incompressible-plastic solid complying with von Mises yield criterion and Drucker's hypothesis,

$$\dot{\sigma}_x = 2\mu[(1 + \alpha - \beta s_x^2)\dot{\varepsilon}_x + (\alpha - \beta s_x s_y)\dot{\varepsilon}_y - \beta s_x s_{xy}\dot{\gamma}_{xy}],$$
$$\dot{\sigma}_y = 2\mu[(\alpha - \beta s_x s_y)\dot{\varepsilon}_x + (1 + \alpha - \beta s_y^2)\dot{\varepsilon}_y - \beta s_y s_{xy}\dot{\gamma}_{xy}], \tag{1.5}$$
$$\dot{\tau}_{xy} = 2\mu[-\beta s_x s_{xy}\dot{\varepsilon}_x - \beta s_y s_{xy}\dot{\varepsilon}_y + (1/2 - \beta s_{xy}^2)\dot{\gamma}_{xy}],$$
$$(1 + \gamma s_z^2)\dot{\sigma}_z = (\nu - \gamma s_x s_z)\dot{\sigma}_x + (\nu - \gamma s_y s_z)\dot{\sigma}_y - 2\gamma s_z s_{xy}\dot{\tau}_{xy},$$

on $\mathcal{H}$ for $t > 0$: here s_x, s_y, s_z, s_{xy} are the normalized stress deviators

$$s_x = (2\sigma_x - \sigma_y - \sigma_z)/(3\sqrt{3}\tau_0), \qquad s_y = (2\sigma_y - \sigma_x - \sigma_z)/(3\sqrt{3}\tau_0),$$
$$s_z = (2\sigma_z - \sigma_x - \sigma_y)/(3\sqrt{3}\tau_0), \qquad s_{xy} = \tau_{xy}/(\sqrt{3}\tau_0),$$

with τ_0 being the octahedral shear stress,

$$\tau_0 = (\sqrt{2}/3)(\sigma_x^2 + \sigma_y^2 + \sigma_z^2 - \sigma_y\sigma_z - \sigma_z\sigma_x - \sigma_x\sigma_y + 3\tau_{xy}^2)^{1/2},$$

and α, β, γ are the material constants

$$\alpha = \nu/(1 - 2\nu), \qquad \beta = \mu/(\mu + \mu_p), \qquad \gamma = (1 + \nu)\mu/\mu_p,$$

with ν being Poisson's ratio, μ the shear modulus and μ_p the plastic octahedral shear modulus defined by $\mu_p = \dot{\tau}_0/2\dot{\varepsilon}_0$, where $\dot{\varepsilon}_0$ is the octahedral plastic strain rate, the analogue of $\dot{\tau}_0$. The *strain-rate/displacement-rate relations* for infinitesimal strain rates,

$$\dot{\varepsilon}_x = \partial\dot{u}/\partial x, \qquad \dot{\varepsilon}_y = \partial\dot{v}/\partial y, \qquad \dot{\gamma}_{xy} = \partial\dot{u}/\partial y + \partial\dot{v}/\partial x, \tag{1.6}$$

on $\mathcal{H}$ for $t > 0$. The *contact conditions* under the rigid cylinder,

$$\dot{v} = \dot{\delta} \tag{1.7}$$

[†] The usual engineering notation for stresses, strains and displacements is employed; here and hereafter a dot atop a quantity indicates the corresponding rate.

on ∂_{1w} for $t > 0$, wherein δ is the prescribed rate of increase of n, constant throughout the contact region, in conjunction with either

$$\dot{u} = 0 \qquad \text{or} \qquad \dot{\tau}_{xy} = 0, \tag{1.8}$$

on $\partial_1\mathcal{H}$ for $t > 0$, the first reflecting adhesive contact (slip completely restrained) while the second approximates lubricated contact (perfectly smooth). The *stress-free conditions* on the remainder of the half-space surface,

$$\dot{\sigma}_y = 0, \qquad \dot{\tau}_{xy} = 0, \tag{1.9}$$

on $\partial_2\mathcal{H}$ for $t > 0$. And, finally the *conditions at infinity* which insist that the stresses remain zero there,

$$\dot{\sigma} = o(1) \qquad \text{as} \qquad x^2 + y^2 \to \infty, \tag{1.10}$$

on $\mathcal{H}$ for $t > 0$.

Several comments concerning the modelling underlying the foregoing formulation are in order. First, the *plane strain approximation* for the half-space is physically representative of indentation by a rigid cylinder away from its ends provided that the cylinder is sufficiently long with respect to its radius and that the indented material has a relatively large bulk and is consistently constrained in the cylinder axial direction. Second, the *quasi-static assumption* is physically reasonable even for dynamic indentation when the duration of the contact is an order of magnitude longer than the time taken for the leading elastic wave front to traverse the contact area.† Third, the simplification of a *rigid* indenter is appropriate when the response of the indented substrate is of interest rather than that of the indenter itself, and is realistic for actual configurations in which the indenter experiences relatively little total deformation. That is, in instances in which there is significant plastic flow in the half-space, when the indenter is sufficiently relatively hard so as not to yield appreciably. Fourth, the usual *inverse approach* is adopted to overcome the geometric nonlinearity caused by the conforming contact, that of not knowing the contact extent *a priori* for a given load; thus $a, \dot{a}$ are in effect set in (1.7) via prescription of $\partial_1\mathcal{H}$ and F backed out. Fifth, an approximation, reasonable for $a^2/R^2 \ll 1$, is involved in the lubricated case in (1.7) and (1.8) where rectangular coordinates are used instead of the local cylindrical coordinates needed for an exact, but less tractable, statement. Last, the intent of the different contact conditions in (1.8) is to bound the effects of *friction*.

Turning to the nature of the problem class at hand, we note that the quasi-static assumption means that, although relationships change with time, they are independent of the time scale. Hence, in essence, we are faced with solving for the nine rate, or incremental, quantities in $\dot{\sigma}, \dot{\varepsilon}, \dot{u}$ as functions of the two variables x, y satisfying the quasilinear system of partial differential equations (1.4)–(1.6) together with the conditions (1.7) through (1.10)—a task almost certainly intractable to any purely analytical approach. Accordingly we look to numerical solution methods in what follows and, to this end, require the specification of the requisite material constants before proceeding further. We choose a single material having elastic moduli $\nu = 0.33$, $\mu = 6 \times 10^3$ ksi (41×10^3 MPa), a uniaxial yield stress of 15 ksi (103 MPa) and a uniaxial stress–strain curve with a strain hardening exponent n of 0.5, i.e. $(\sigma/\sigma_Y) = (\varepsilon/\varepsilon_Y)^n$ for $\varepsilon \geqslant \varepsilon_Y$, wherein σ, ε are uniaxial true stress, strain and σ_Y, ε_Y their respective values at yield. Thus μ_p is provided in effect by the $\sigma - \varepsilon$ curve and the limiting value of the octahedral stress implicit in the definition of μ_p, τ_Y, set at 32 ksi (220 MPa). The choice of $n = 0.5$ represents a computationally convenient middle value between elastic ($n = 1$) and perfectly plastic ($n = 0$) response.‡ While the other material constants selected

---

† This is essentially an adaptation of Love's criterion ([8], Section 139).

‡ Some additional calculations were performed for $n = 0.1$. Unfortunately the numerical noise levels for these computations were high enough so as to raise questions about their quantitative significance; qualitatively though the results were similar to those found for $n = 0.5$.
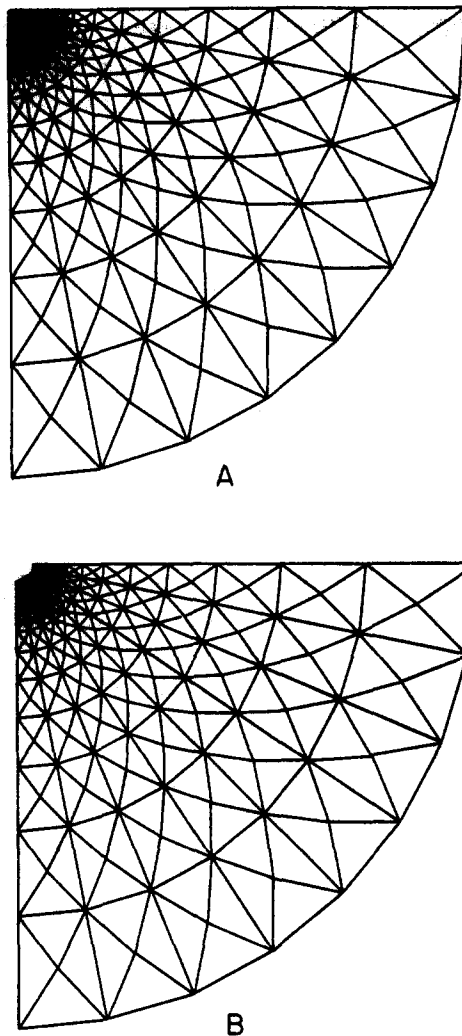
Fig. 2. Finite element grid : (A) inner region ; (B) outer region.

stem from a related experimental program on a specific copper alloy, it is hoped that subsequent suitable nondimensioning limits the dependency on their particular values for the most part. With these details in place we now move on to the solution technique to be used.

The quasilinear nature of the governing equations in the preceding formulation aids in establishing an energy principle for the incremental field quantities of elasto-plastic flow. This principle forms a natural basis for finite element methods (FEM) and several codes exist which implement this type of FEM (see, e.g. [9]). Underlying the approach in these codes is the discretization of the continuum entailed. Basically the issues encountered in this process for the present problem are dealt with in the axisymmetric counterpart by Follansbee and Sinclair[7], so that we merely summarize the main points here.†

The expected continuity of the fields motivates the choice of constant strain triangles as the elements in the analysis, while the symmetry involved allows attention to be confined to the quarter plane $x \geqslant 0$, $y \geqslant 0$. Within this quarter plane, a finite circular quadrant for discretization is taken so that the infinity conditions are complied with to within $\sim 2\%$. The actual element grid is then constructed in an *ad hoc* fashion so as to aid resolution with element size gradation, to retain locally a nearly isotropic arrangement, and to keep computational effort within sensible bounds; the compromise arrived at to this effect has 722 elements with 391 nodes or 782 degrees of freedom (Fig. 2). We start the analysis with

† Greater detail of the analysis may also be found in Cinar[10].

the elastic deformation which is applied in a single increment having eleven nodes in contact. Thereafter, indentation is increased steadily by a factor λ, that is $\delta = \lambda\delta$ in (1.7) ($\lambda = 0.05$ typically). Hence the extent a itself increases, and we must check the next node outside the contact region to discern when it comes in contact; usually an iteration is required to adjust the magnitude of the last δ so that the node just comes into contact, and we know the new indentation extent exactly at that point. Rather than continue this procedure until the next node is contacted, we now scale the grid such that the contact region returns to one with eleven nodes in contact, then repeat the expansion as indentation proceeds. This last is the expansion technique used in Follansbee and Sinclair[7] and is computationally efficient in maintaining the initial resolution of the grid.

The foregoing analysis admits to some *checks*. At the outset we can compare answers with their exact elastic counterparts given by Poritsky[3] after Hertz[2] for lubricated contact and Cinar[10], Appendix B, for adhesive contact. As plastic flow commences though, no exact elasto-plastic solution appears to be available for validating our approach. Nonetheless, by setting δ equal to 0.05δ, 0.025δ and 0.0125δ, convergence with load increment can be checked. Another check of sorts for low load levels can be made by comparing the lubricated contact problem with the analysis of Dumas and Baronet[6]. Ultimately, we take the analysis forward until we have no direct analytical checks, and the response for both lubricated and adhesive contact conditions becomes fully plastic. With the analysis checked where possible and these latter calculations made, a variety of results of physical import bear examination, but before we can make this review we need to reduce the vast amount of data generated by our approach. We look to a means for facilitating this task next.

As mentioned earlier, we use constant-strain-triangle elements in our FEM map. As a result, elemental quantities such as stresses, strains, etc., are assigned to the centroids of the triangles each of which sees a different surrounding pattern of elements in its immediate vicinity. This lack of local isotropy in the element arrangement is believed to promote the significant element-to-element variations experienced as plastic flow progresses. Certain of the nodes, on the other hand, see a nearly isotropic array of elements right about them, e.g. those at the centers of "union jacks" in Fig. 2. Consequently we estimate stresses and the like as simple nodal averages weighted as the inverse of the distance between surrounding centroids and the node in question (see Cinar[10] for the actual formula for this averaging). We find that this data reduction scheme inhibits extraneous fluctuations considerably. Even so, some numerical noise persists, most noticeably in the contact stresses. Thus we smooth the normal contact stress by fitting it with

$$\sigma_y/p = \{C_1[1 + C_2(x/a)^2]\sqrt{(1-(x/a)^2)}\}U(1-x/a), \qquad (1.11)$$

where $p = F/2a$ is the average contact pressure, C_1, C_2 are the constants to be adjusted, and U is the unit step function. The form of (1.11) owes its origin to the stress-free condition outside the contact region, to σ_y's elastic predecessor, and to the fact that σ_y is an even function of y. The determination of C_1, C_2 in (1.11) is carried out by first ensuring the correct average value is recovered on integration and thereafter fitting the data in a least squares sense. For the other stress components in the contact area it is not so clear what are reasonable functions to fit. Thus we circumvent the difficulty somewhat by giving these components at nodes near but not at the surface, since there is less noise at such stations by virtue of having complete clusters of elements about nodes for the averaging. For these results and all others we merely use hand-drawn fits with a French curve to obtain smooth plots.

While these smooth curves possess the advantage of removing the distracting high-frequency oscillations present in the underlying data—an especially attractive feature when displaying a number of curves in a single figure to show trends, etc.—it is nonetheless important to preserve some idea of the extent to which the results presented are subject to numerical noise. With this in mind we introduce the *standard deviation* s calculated in accordance with

$$s = \sqrt{\Sigma(f_d - f_f)^2/N}, \qquad (1.12)$$

where N is the total number of data points fitted and f_d, f_f are values of the field quantity of interest taken from the data and the corresponding point on the fitted curve, respectively. The standard deviation of (1.12) is calculated for each quantity in the figures that follow and the s so found tabulated in the Appendix. From these values the reliability of the results given may be inferred, even if only in an informal fashion. Summarizing the standard deviations of the Appendix in this way, we can see that the results presented really do not suffer much from numerics.† We look to review the implications of these results next.

2. RESULTS AND DISCUSSION

In this section we start by discussing those aspects of our analysis which enable the approach to be verified to a degree. We then consider how best to nondimensionalize findings prior to presenting results showing the indentation extent with increasing pressure, contact and interior stresses for different load levels and their corresponding residual fields, yield region growth, and relative displacement profiles of the surface.

We begin our examination of validating results with the *elastic stresses*. We expect errors to be greater in the stresses (or strains) rather than the displacements, because of their relatively slow convergence in FEM, and accordingly that the accuracy of the stress determinations constitutes the most stringent check on our elastic analysis. For the smooth case using the exact solution in Portisky[3], we find that errors on the axis of symmetry for the axial stress component σ_y as a percentage of the average pressure p are uniformly less than 1.2% and typically of the order of 0.7%, while in the contact region the maximum value of the same error measure for the contact stress σ_y (without any smoothing) is less than 1.8% with an average value of 0.5%.‡ For the adhesive case the exact solution (Cinar[10], Appendix B) on the axis of symmetry shows that the transverse normal stress σ_x is about half of the axial normal stress σ_y at the origin, whereas in the smooth solution σ_x equals σ_y at the origin. As a result we look at the errors in both quantities; we find that the FEM analysis picks up the change with the errors in both stress components being very similar to those for the smooth instance on the symmetry axis. The exact solution for the elastic adhesive problem in addition shows that the contact stresses are *singular* at the edge of the contact region, the normal contact stress σ_y changing sign and becoming tensile at $x/a = 0.97$, the shear stress τ_{xy} changing sign at a somewhat larger value of x/a, then both stresses oscillating in a very small strip near the edge of the contact region with their magnitudes approaching infinity as $x/a \rightarrow 1$. This sort of elastic singularity in *conforming*, adhesive, contact problems, when the indentation is applied in a single step as here, can be also observed in the axisymmetric problem—see Spence[12], p. 67—and serves notice that we can only draw physical inferences for this contact condition from either stresses/strains away from the edge of the contact region or integrated quantities such as mean pressures, displacements, etc. To the extent our FEM grid provides information on this activity, the results agree with these anomalous analytical findings, the errors in both σ_y and τ_{xy} being at most 7% of p and generally less than 1.7% for $x/a \leq 0.91$.

Turning to the elastoplastic aspect of our analysis, we check *convergence with load increment* δ. The result displaying the greatest sensitivity to load step proves to be the normal contact stress σ_y. For lubricated contact, loading till a load per unit length an order of magnitude greater than that required to initiate yield gives rise to a maximum difference in σ_y of 0.5% as δ is reduced from 0.05δ to 0.025δ, and to a maximum difference of 0.2% as $\delta = 0.025\delta \rightarrow 0.0125\delta$. In the light of this small dependence on the choice of load increment and in the interests of keeping computation to a minimum, we set δ equal to 0.05δ in all subsequent analysis.

---

† By way of comparison, the standard deviations here are typically significantly smaller than the corresponding one for the same type of analysis of the spherical indentation problem (refer Sinclair *et al.*[11]). This is probably due largely to the lower stress gradients present initially in the plane strain problem relative to the axisymmetric (as with the Flamant line load cf. the Boussinesq point load).

‡ Further details of this and all other checks may be found in Cinar[10], which also contains a demonstration of convergence for the smooth elastic problem on a sequence of three successively more refined grids which culminate in the FEM map of Fig. 2.

Preliminary to comparing the present analysis with that of Dumas and Baronet[6], we seek a means of nondimensionalizing results so that those for our specific material reflect general trends as much as possible. Thus we look for the analogue of the *flow stress*, or representative yield stress, introduced by Tabor[13] to combine the fully plastic responses to spherical indentation for many materials into one. In Tabor[13], for strain-hardening materials this flow stress σ_f is shown experimentally to be that occurring near the edge of the indentation if the relationship for nonhardening materials ($\sigma_f \equiv \sigma_Y$) is to be preserved, namely

$$p \simeq 2.8\sigma_f, \tag{2.1}$$

where p for the sphere is the average contact pressure or Meyer hardness. The associated uniaxial strain, ε_f, is empirically related to the indentation extent as in

$$\varepsilon_f = 20a/R, \tag{2.2}$$

where ε_f is in percent and a, which is for the sphere, is the contact circle radius. In Cinar[10], analogous numerical experiments for cylindrical indentation are performed. These demonstrate that there is a marked sensitivity as to just where at the edge of the contact region one picks as representative concerning whether or not (2.2) holds—near surface nodes with a/R equal to 0.95, 0.99 and 1.09 give ε_f as 32, 24 and 7 times a/R, respectively, for frictionless contact, with like results for adhesive. Taking ε_f as $20a/R$ then, just as Tabor, we have

$$\sigma_f = \begin{cases} \sigma_Y(\varepsilon_f/\varepsilon_Y)^n & \text{if} \quad \varepsilon_f = 20a/R \geqslant \varepsilon_Y, \\ \sigma_Y & \text{otherwise,} \end{cases} \tag{2.3}$$

when the strains are expressed in percentages. For this flow stress we find for cylindrical indentation that (2.1) is replaced by

$$p \simeq 2.24\sigma_f, \tag{2.4}$$

irrespective of contact condition.

The fundamental overall response in our study is the indentation extent for varying indentation pressure or "hardness". The pressure can be normalized by σ_f of (2.3); needed is a way of nondimensionalizing the indentation extent. In filling this need we follow the approach, first suggested by Johnson[14] and subsequently developed in Sinclair *et al.*[11], for spherical indentation. We take, as our dimensionless measure of indentation extent $\bar{a}$,

$$\bar{a} = aE_r/R\sigma_Y. \tag{2.5}$$

Here E_r is a representative Young's modulus for contact accompanying a representative Poisson's ratio v_r, which is a weighted average between its elastic value v and its plastic value of 0.5, viz.,

$$E_r = \frac{E}{1-v_r^2}, \qquad v_r = \begin{cases} \frac{1}{2}[1-(\varepsilon_Y/\varepsilon_f)(1-2v)] & \text{if} \quad \varepsilon_f \geqslant \varepsilon_Y, \\ v & \text{otherwise.} \end{cases} \tag{2.6}$$

This choice of $\bar{a}$ offers several advantages. First, it renders all elastic responses material insensitive since the corresponding exact solution has $p/\sigma_f = p/\sigma_Y = Ea/8(1-v^2)\sigma_Y R = \pi\bar{a}/8$. Second, it recovers (2.4) for our analysis at very large indentations. Third and final, it allows the elastic result to be interpreted approximately as an elasto-plastic one for a material with an initial yield stress of σ_Y and a strain-hardening exponent of $n = 1$. This last leads to a limiting value of p/σ_f of 2.62 as $\bar{a} \to \infty$, in fair agreement with (2.4). Using the normalizing flow stress of (2.3) and the dimensionless indentation $\bar{a}$ of (2.5), our curve of indenting
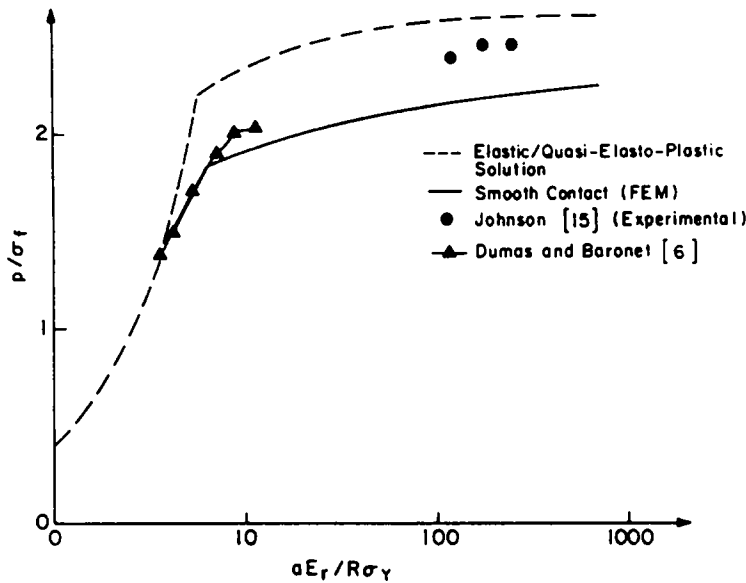
Fig. 3. Hardness dependence on indentation extent.

pressure or hardness versus indentation extent is given in Fig. 3 for the frictionless contact condition, together with the quasi-elasto-plastic interpretation of the elastic solution. The corresponding curve for adhesive contact is indistinguishable from the smooth one on the scale of Fig. 3 so that *friction effects* do not appear to play a major role here.

In the spherical counterpart to Fig. 3 in Sinclair *et al.*[11], the response is classified into three regimes: the *elastic* at low load levels where there is no yielding, the *fully plastic* at high loads which induce a steady state of sorts, and the *elasto-plastic* at intervening pressures. The demarkation between the first and third for the present problem is clear and is computed to occur at

$$p/\sigma_f = 1.37, \qquad aE_r/R\sigma_Y = 3.5. \tag{2.7}$$

However, the point separating the second and the third is far less obvious and raises questions as to the very existence of a fully plastic regime for cylindrical indentation. Simply for the convenience of loosely categorizing response in the following discussion, we pick

$$p/\sigma_f = 2.12, \qquad aE_r/R\sigma_Y = 80, \tag{2.8}$$

as the boundary between the elasto-plastic and fully plastic regimes in our analysis. The same point in terms of indentation extent gives $p/\sigma_f = 2.56$ for our quasi-elasto-plastic solid, so that we can expect material dependence in the hardness at this boundary.

Also shown in Fig. 3 are comparisons with *other investigations*. In the elasto-plastic regime we compare our results with the FEM analysis of Dumas and Baronet[6]. The agreement is good up to the greatest dimensionless indentation extent treated in [6] of about 11. In the fully plastic regime we compare with the experiments of Johnson[15]. The highest hardness in [15] is $p/\sigma_f = 2.45$ compared to our 2.24 (from FEM) and 2.62 (from quasi-elasto-plastic). Hence our results bracket the empirical but differ from it by about ±8% in contrast to the very close agreement for all three in the spherical instance. Whether this variation is something that would be reduced by an improved finite element analysis with a refined grid, or whether it is inherent in cylindrical indentation, is an open question; probably the answer is both to some degree. Consequently for indenting cylinders the flow stress does not appear able to reduce the results for all material hardnesses in the fully plastic regime to a single dimensionless value. Even so it would seem that σ_f remains the best nondimensionalizing stress for use in the presentation of stress results which we turn to next.
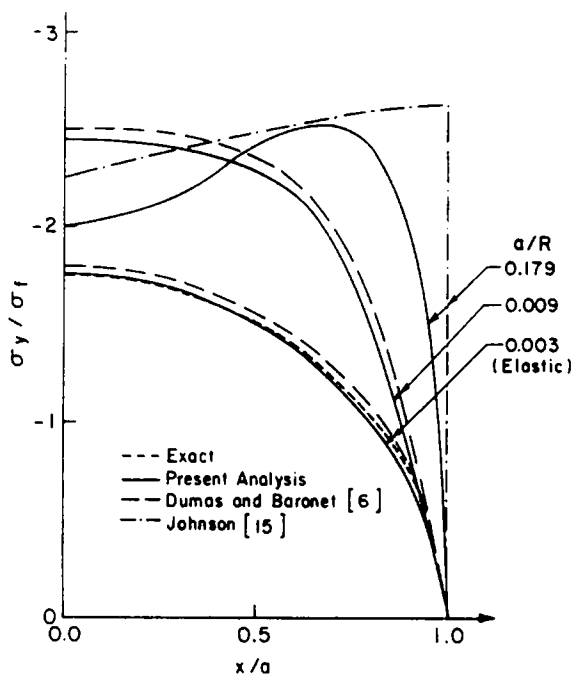
Fig. 4. Comparison of contact pressure with related analyses and experiments.

We commence our presentation with the *contact stresses*. In Fig. 4 we compare the dimensionless normal contact stress from our frictionless analysis, σ_y/σ_f, as a function of the transverse coordinate x/a, with other analyses and experimental results. The comparison between Dumas and Baronet[6] and our finite element analyses with Hertz's elastic solution at the point of yield ($a/R = 0.003$) shows that the present results are slightly closer to the exact solution. In the elasto-plastic regime ($a/R = 0.009$) we make a second comparison with Dumas and Baronet[6], while in the fully plastic regime ($a/R = 0.179$) we compare with Johnson's experimentally inferred results[15]. Both comparisons represent good agreement. A feature of the latter is that both the analytical and the empirical determination show a nearly uniform contact pressure distribution at high indentation. In this connection too we note that if we continue to interpret the elastic solution as a quasi-elasto-plastic response but modify it by replacing the classical parabolic approximation to the indenter profile with its exact expression which is more appropriate for large indentations, we find that the pressure distribution approaches a uniform one as $a/R \to 1$ (refer to Cinar and Sinclair[16]). In Fig. 5 we exhibit the normal contact stress for a sequence of indentations. We focus on the smooth contact condition because of the elastic singularity present in the adhesive instance described earlier, a policy we continue hereafter, and limit presentation to a set of four, different, post-yield load levels which we judge to be sufficient to show trends. These loads correspond to early in the elasto-plastic regime, in the middle of the elasto-plastic regime, early in the fully plastic regime and well into the fully plastic regime. Details are given in Table 1 where F_Y is the load per unit length computed to just induce yielding in the half-space; in what follows we distinguish corresponding curves by their values of a/R taken from the first column of Table 1. Figure 5 then displays σ_y, normalized by σ_f, as a function of x/a for the four levels of indentation in Table 1 together with the results for on the point of yield ($a/R = 0.003$). The transition from elastic to elasto-plastic response shows some flattening of the pressure distribution which later continues to the point that the contact pressures exhibit some rising towards the edge of the contact region. Observe also that, while the difference between the two fully plastic responses is less than earlier changes for comparable increments in a/R, it is not obvious that a steady state is reached even at the highest indentation.

Near-surface interior stresses are displayed in Fig. 6(A) which shows the frictionless stress components σ_y, σ_x, normalized by the flow stress σ_f, along a ray emanating from the
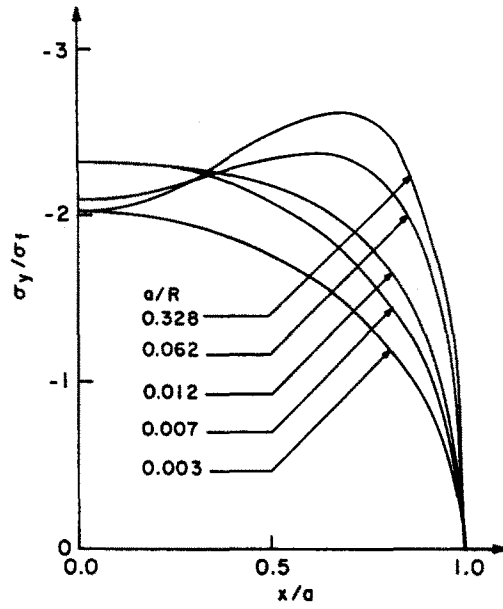
Fig. 5. Frictionless contact pressure distributions.

Table 1. Indentations selected for frictionless contact

Indentation extent		Flow stress	Load levels	
a/R	$aE_r/R\sigma_Y$	σ_f/σ_Y	p/σ_f	F/F_Y
0.0067	8	1.19	1.88	4
0.0117	15	1.58	1.98	9
0.0620	86	3.62	2.12	118
0.3280	462	8.34	2.24	1520
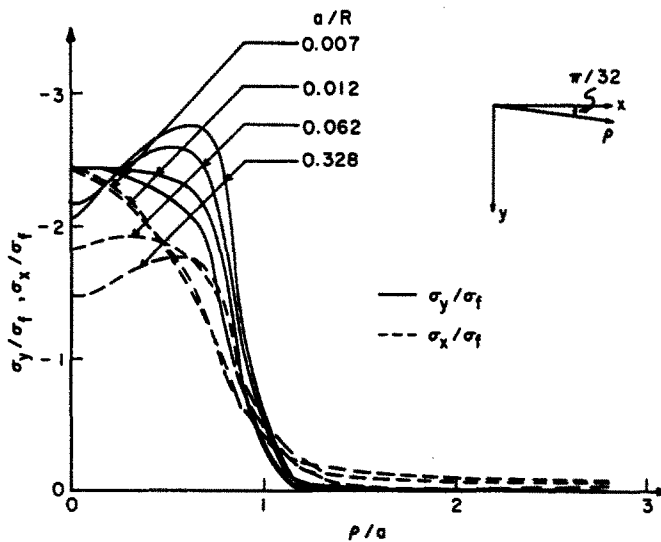
Fig. 6(A). Interior stress distributions: near surface.
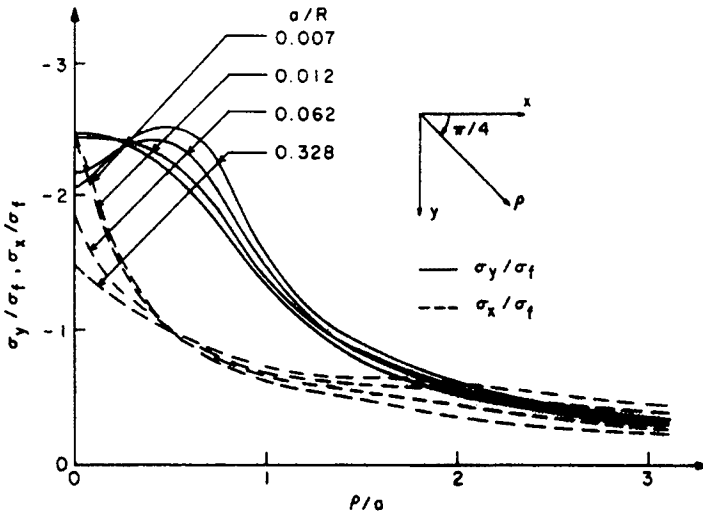
Fig. 6(B). Interior stress distributions: along a 45° ray.

origin at an angle of $\pi/32$ below the surface, as a function of ρ/a, where $\rho = (x^2 + y^2)^{1/2}$ is the distance from the origin. Several comments are in order. For the elasto-plastic results, the two stress components continue to remain nearly equal, as they are for the initial elastic response, at $\rho = 0$. Later on as indentation proceeds, $|\sigma_x| = 0.7|\sigma_y|$; this result is quite comparable to that deduced from experiments by Johnson[15] which has $|\sigma_x| = 0.6|\sigma_y|$ at the origin. Both stress components decay rapidly around $\rho/a = 1$ and become nearly zero when $\rho/a > 1$. There is no evidence of tensile stresses just out from under the contact region (cf. spherical indentation in Sinclair et al.[11]). Again results for the higher indentations are similar but do not really support the existence of a single steady-state distribution.

Stresses deeper within the interior are given in Fig. 6(B) which presents the frictionless σ_y, σ_x stress components, nondimensionalized by the flow stress, along a ray inclined at $\pi/4$ to the upper surface. Generally, $|\sigma_x|$ is less than $|\sigma_y|$, and both stresses decay less abruptly
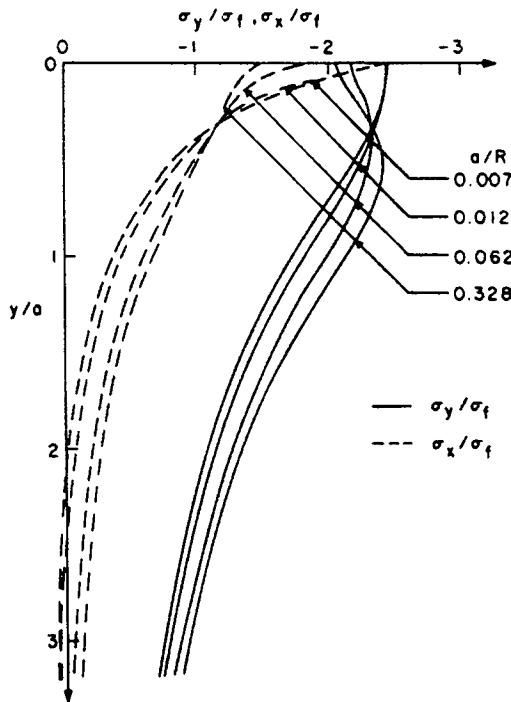

Fig. 6(C). Interior stress distributions: on axis of symmetry.

as p/a gets larger. Responses within the fully plastic regime are quite similar but not close to identical.

Frictionless *stresses down the axis of symmetry* are furnished in Fig. 6(C). Here we observe that, in the fully plastic regime, σ_y displays a subsurface maximum, a feature common in contact problems, and reaches a peak value about $p/a = 0.5$. There are indications of this type of phenomena for σ_y in the experimentally inferred distribution in Johnson[15]. The σ_x component decays far faster than the σ_y leaving the latter as markedly dominant. The experimental study of Johnson[15] does not agree with this finding for the limited depths considered there $(0 \leqslant y/a < 0.8)$, though the more rapid decay in σ_x at greater depths is consistent with expectations from an application of St. Venant's principle. As this location is well away from the singular point in the adhesive analysis, some comparisons are reasonable. For σ_y there is little to distinguish between the two contact conditions, while for σ_x the initial elastic difference remarked on previously almost disappears by the time the fully plastic response is attained (see Cinar[10] for further details). All responses in the fully plastic regime are reasonably close.

Turning to the *residual stress distributions* we start by considering the possibility of *reverse plastic flow on unloading*. We do this by adapting Johnson's argument[17] to reflect the fact that our contact pressure is constant throughout the contact region in the fully plastic regime to all intensive purposes and that we have a plane strain situation. We find that the possibility of reverse plastic flow is far less here than for the axisymmetric case. This is partly because the elastic solution (see, e.g. Muskhelishvili[18], §93a) to be subtracted off supplies a lower maximum difference in principal stresses, but is mainly due to the pressure being removed being a smaller multiple of the flow stress (recall that $p = 2.24\sigma_f$ at most here instead of 2.8). As a consequence we simply obtain residual stresses from our frictionless analysis by subtracting the elastic stress response to a uniformly loaded strip. The resulting distributions are shown in Fig. 7.

The first of such figures, Fig. 7(A), displays the *near-surface residual stress* distributions for σ_x—the other component σ_y is comparatively negligible. Unloading from the elasto-plastic regime leads to a small compressive region around the origin while unloading from the fully plastic gives rise to tensile stresses there. Near the limit of the contact region $(p/a \simeq 1)$, all residual stresses are tensile. Figure 7(B) presents *residual stresses on an intervening ray* between those of Fig. 7(A) and the *axis of symmetry*, the latter having residual stresses as drawn in Fig. 7(C). In these two figures we include σ_y for unloading from the three higher levels of indentation in Table 1 but omit it from the lower since again it is relatively small. In both figures the residual σ_x is tensile in the vicinity of the origin before changing sign to become compressive. Qualitatively similar tensile σ_x are estimated in Johnson[15]. All stresses ultimately decay towards zero as p/a, $y/a \to \infty$. Hence it is not surprising to see
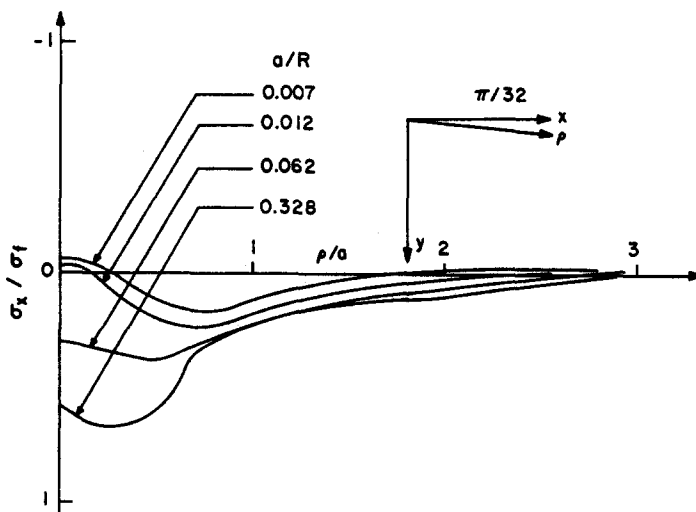

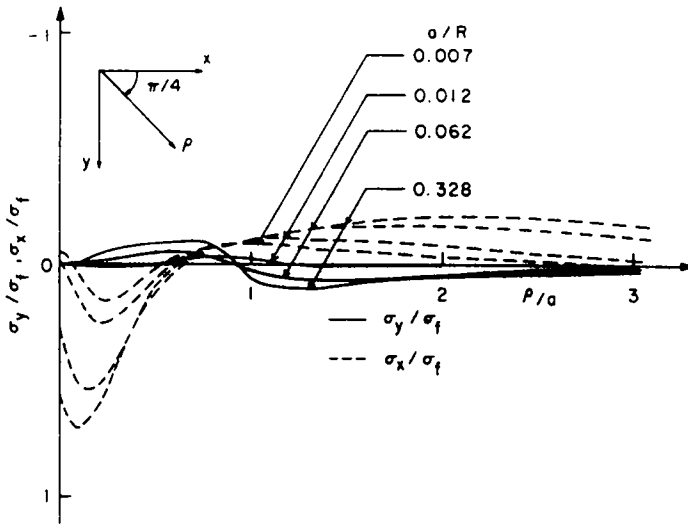Fig. 7(A). Residual stress distributions: near surface.

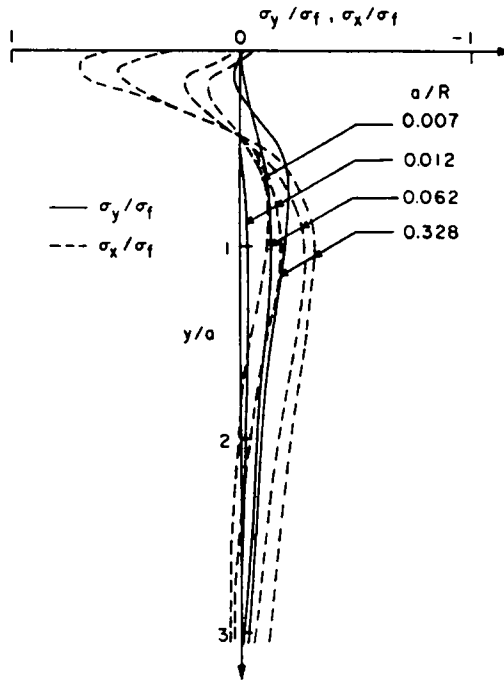Fig. 7(B). Residual stress distributions: along a 45° ray.

Fig. 7(C). Residual stress distributions: on axis of symmetry.

that $|\sigma_y|$ is smaller than $|\sigma_x|$ for all curves, given that the free surface remaining on unloading insists σ_y start at zero at $p/a = y/a = 0$. Qualitatively this ordering of stress component magnitudes may be seen in Johnson[15] too.

Now considering the *deformations* that accompany the foregoing stresses, we begin by viewing the regions of yielded material under our selected loads for the frictionless contact condition (Fig. 8).† In Fig. 8, the partial sectioning indicates the side of the elastic-plastic boundary on which the material is yielded, and the portion of the yield region boundary nearest the origin is only associated with the lowest load level ($a/R = 0.007$). We expect this elastic enclave early in the elasto-plastic regime because first yielding occurs on the axis of symmetry at a depth of about $y/a = 0.75$, and the contact region is in a state of near hydrostatic pressure ($\sigma_x = \sigma_z = 1.52\sigma_z$, $\tau_{xy} = 0$) for the initial elastic loading. Thus the yield

---

† Plastic strain distributions in the fully plastic regime are available in Cinar[10].
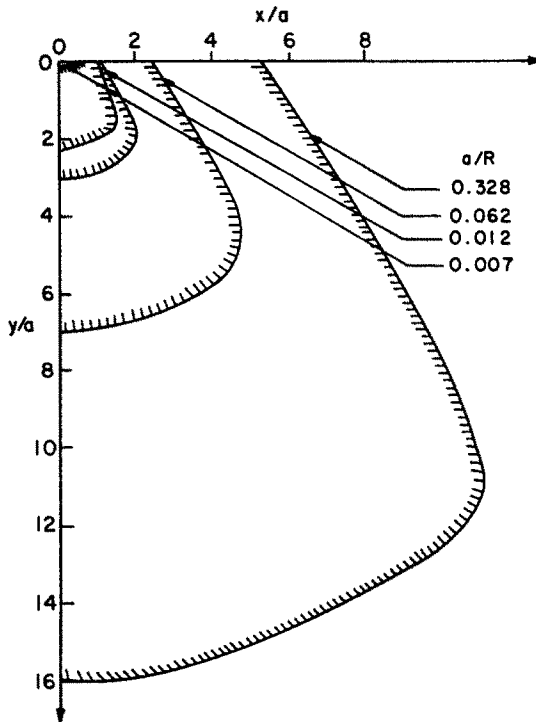
Fig. 8. Yield regions.

region grows towards the rigid cylinder as well as down into the half-space at the outset. The yield region grows significantly faster in depth than in lateral extent. This is in marked contrast to the analytical findings of Sinclair *et al.*[11] and the experimental determinations of Samuels and Mulhearn[19] for the sphere, which have highly comparable extents in both directions, apparently approaching a limiting value between 4 and 5 times the contact radius. This difference can perhaps be attributed to the different rates of decay with depth for the stresses in the plane strain and axisymmetric, elastic, concentrated, load problems— $(y/a)^{-1}$ as opposed to $(y/a)^{-2}$. It would seem as a result that the depth of the yield region under a cylindrical indenter is not asymptotic to a bounding value, and this lack of a limit may well contribute to the less than convincing demonstration of steady state response in the fully plastic regime for other results.
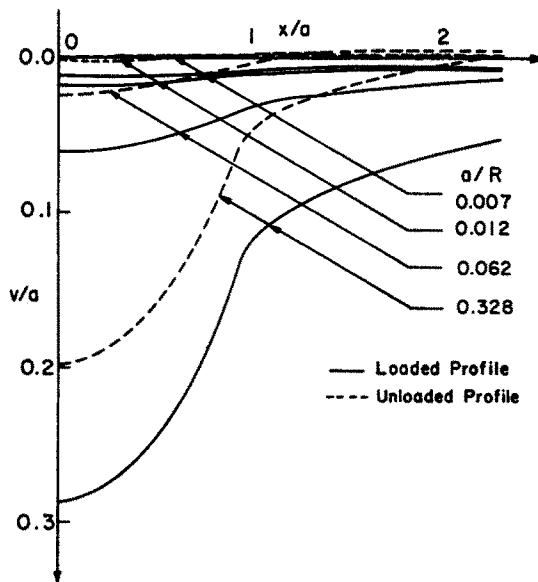

Fig. 9. Relative surface displacement profiles.

As our final set of curves, an enlarged view of *displacment profiles* is provided in the non-cartesian plots of Fig. 9. For the two-dimensional problem, absolute displacement values are meaningless; somewhat arbitrarily those of Fig. 9 are made relative to a point on the surface at a distance of $40a$ from the origin. On unloading (broken lines in Fig. 9), some "shallowing-up" is indicated in the depth of impression, but little if any effect on its extent is discernible—this sort of response for spherical indentation is observed by Tabor in [13].

In sum, the present analysis would seem to have captured the physical response to cylindrical indentation sufficiently to agree reasonably well with the available physical evidence, and to allow physically meaningful inferences to be drawn at high load levels.

REFERENCES

1. P. S. Follansbee, G. B. Sinclair and J. C. Williams, Modelling of low velocity particulate erosion in ductile materials by spherical particles. *Wear* **74**, 107 (1981).
2. H. R. Hertz, *Miscellaneous Papers*. English trans. Macmillan, London (1896).
3. H. Poritsky, Stresses and deflections of cylindrical bodies in contact with application to contact of gears and locomotive wheels. *J. appl. Mech.* **17**, 191 (1950).
4. I. F. Collins, A simplified analysis of the rolling of a cylinder on a rigid/perfectly plastic half-space. *Int. J. mech. Sci.* **14**, 1 (1972).
5. R. Hill, *The Mathematical Theory of Plasticity*. Clarendon, Oxford (1950).
6. G. Dumas and C. N. Baronet, Elastoplastic indentation of a half-space by an infinitely long rigid circular cylinder. *Int. J. mech. Sci.* **13**, 519 (1971).
7. P. S. Follansbee and G. B. Sinclair, Quasi-static normal indentation of an elasto-plastic half-space by a rigid sphere—I. Analysis. *Int. J. Solids Struct.* **20**, 81 (1984).
8. A. E. H. Love, *A Treatise on the Mathematical Theory of Elasticity*, 4th Edn. Dover, New York (1944).
9. J. L. Swedlow, A procedure for solving problems of elasto-plastic flow. *Comput. Struct.* **3**, 879 (1973).
10. A. Cinar, Quasi-static normal indentation of an elasto-plastic half-space by a long rigid cylinder. Ph.D. Dissertation, Carnegie-Mellon University, Pittsburgh (1984).
11. G. B. Sinclair, P. S. Follansbee and K. L. Johnson, Quasi-static normal indentation of an elasto-plastic half-space by a rigid sphere—II. Results. *Int. J. Solids Struct.* **21**, 865 (1985).
12. D. A. Spence, Self similar solutions to adhesive contact problems with incremental loading. *Proc. R. Soc. (Lond.)* **A305**, 55 (1968).
13. D. Tabor, *The Hardness of Metals*. Clarendon Press, Oxford (1951).
14. K. L. Johnson, The correlation of indentation experiments. *J. Mech. Phys. Solids* **18**, 115 (1970).
15. K. L. Johnson, An experimental determination of the contact stresses between plastically deformed cylinders and spheres. *Engineering Plasticity*, p. 341. Cambridge University Press (1968).
16. A. Cinar and G. B. Sinclair, Large indentation of an elastic half-space by an infinitely long rigid cylinder. Report SM 83-18, Dept. of Mechanical Engng, Carnegie-Mellon University, Pittsburgh (1983).
17. K. L. Johnson, Reversed plastic flow during the unloading of a spherical indenter. *Nature* **199**, 1282 (1963).
18. N. I. Muskhelishvili, *Some Basic Problems of the Mathematical Theory of Elasticity*, 4th Edn. Noordhoff Groningen, The Netherlands (1963).
19. L. E. Samuels and T. O. Mulhearn, An experimental investigation of the deformed zone associated with indentation hardness impressions. *J. Mech. Phys. Solids* **5**, 125 (1956).

APPENDIX

Here we record (Table 2) the standard deviation s of (1.12) for all the curves in Figs. 3–9 which do not pas through every data point ($s = 0$ for curves that do). All of these curves have the same number of data points $N = 16$.

Table 2. Numerical noise levels in results presented

Source Figure	a/R value	Standard deviations s in σ_y/σ_f	s in σ_x/σ_f
6(A)	0.012	0.02	0.00
	0.062	0.05	0.01
	0.328	0.08	0.02
6(B)	0.328	0.01	0.05
6(C)	0.328	0.01	0.04
7(A)	0.062	0.00	0.01
	0.328	0.00	0.01
7(B)	0.328	0.01	0.01